

Article

Sustainable Waste Tire Derived Carbon Material as a Potential Anode for Lithium-Ion Batteries

Joseph S. Gnanaraj ^{1,*}, Richard J. Lee ¹, Alan M. Levine ¹, Jonathan L. Wistrom ², Skyler L. Wistrom ², Yunchao Li ³, Jianlin Li ⁴ , Kokouvi Akato ⁵, Amit K. Naskar ⁵ and M. Parans Paranthaman ^{3,*}

¹ Energy Division, RJ Lee Group, 350 Hochberg Road, Monroeville, PA 15146, USA; RLee@RJLeeGroup.com (R.J.L.); ALevine@rjleegroup.com (A.M.L.)

² Practical Sustainability, 1402 N College Drive, Maryville, MO 64468, USA; jonathanwistrom@yahoo.com (J.L.W.); sky_wistrom@hotmail.com (S.L.W.)

³ Chemical Sciences Division, Oak Ridge National Laboratory, Oak Ridge, TN 37831, USA; yli107@utk.edu

⁴ Energy & Transportation Science Division, Oak Ridge National Laboratory, Oak Ridge, TN 37831, USA; lij4@ornl.gov

⁵ Materials Science & Technology Division, Oak Ridge National Laboratory, Oak Ridge, TN 37831, USA; kakato@utk.edu (K.A.); naskarak@ornl.gov (A.K.N.)

* Correspondence: JSGnanaraj@gmail.com (J.S.G.); paranthamanm@ornl.gov (M.P.P.); Tel.: +1-860-405-4914 (J.S.G.); +1-865-574-5045 (M.P.P.)

Received: 17 July 2018; Accepted: 7 August 2018; Published: 10 August 2018



Abstract: The rapidly growing automobile industry increases the accumulation of end-of-life tires each year throughout the world. Waste tires lead to increased environmental issues and lasting resource problems. Recycling hazardous wastes to produce value-added products is becoming essential for the sustainable progress of society. A patented sulfonation process followed by pyrolysis at 1100 °C in a nitrogen atmosphere was used to produce carbon material from these tires and utilized as an anode in lithium-ion batteries. The combustion of the volatiles released in waste tire pyrolysis produces lower fossil CO₂ emissions per unit of energy (136.51 gCO₂/kW·h) compared to other conventional fossil fuels such as coal or fuel–oil, usually used in power generation. The strategy used in this research may be applied to other rechargeable batteries, supercapacitors, catalysts, and other electrochemical devices. The Raman vibrational spectra observed on these carbons show a graphitic carbon with significant disorder structure. Further, structural studies reveal a unique disordered carbon nanostructure with a higher interlayer distance of 4.5 Å compared to 3.43 Å in the commercial graphite. The carbon material derived from tires was used as an anode in lithium-ion batteries exhibited a reversible capacity of 360 mAh/g at C/3. However, the reversible capacity increased to 432 mAh/g at C/10 when this carbon particle was coated with a thin layer of carbon. A novel strategy of prelithiation applied for improving the first cycle efficiency to 94% is also presented.

Keywords: battery grade carbon; waste tires; lithium-ion batteries; pouch cells; disordered carbon microstructure; surface coating

1. Introduction

Rechargeable lithium-ion batteries (LIBs) are being used as the most promising power source for small-scale applications such as consumer portable electronics, power tools and large-scale applications such as advanced power load leveling for smart grids to meet the energy demands of modern mobile technology, electric vehicles (EVs), and hybrid electric vehicles (HEVs) [1]. Graphite is the most widely used anode material due to its high thermal and chemical stabilities, and the practical reversible specific capacity reaching closer to the theoretical capacity of 372 mAh/g corresponding to a fully

lithiated stoichiometric LiC_6 compound [2]. Currently, graphite is being used as an anode in LIBs that powers electric vehicles such as Tesla Model S [3,4]. However, fast charging LIBs pose safety concerns due to lithium plating on the surface of the graphite anode leading to the formation of lithium dendrites, causing inner short-circuiting and capacity fading [5].

Other types of carbonaceous materials such as hard carbons (HCs) and soft carbons (SC) have been investigated as alternate anode materials to enhance the performance characteristics of LIBs [4]. The unique amorphous structure in SC enables fast charging in LIBs even when the micron-sized particles are used, but it suffers from very low specific capacity of 250 mAh/g. The disordered structure in HC is a short-range order which cannot be graphitized even upon high temperature treatments [6]. Hard carbon is less susceptible to exfoliation due to the random orientation of the small graphitic grains. The nanovoids present between the grains reduce isotropic volume expansion. Thus, nanovoids and defects provide additional gravimetric capacity, allowing the capacity to exceed the theoretical capacity of graphite. HCs have demonstrated the ability to store more lithium than graphite and do not exfoliate during repeated cycling in LIBs [7]. Together, these properties make HCs a high capacity high cycle life material. Nevertheless, it suffers from large irreversible capacity loss, which is generally attributed to the high surface area, exposed edge planes in high fraction that increase the absolute quantity of solid electrolyte interphase (SEI) formed, reducing the coulombic efficiency in the first few cycles, and voltage hysteresis [8]. The first cycle irreversible capacity loss in LIBs has been studied extensively and is attributed to the formation of a passivating SEI during the first lithiation process, due to the electrolyte reduction at the negatively polarized graphite surface and the deposition of a number of organic and inorganic compounds, trapping lithium irretrievably in the inner pores of carbon, through chemical bonding with surface functional groups or by reaction with adsorbed oxygen/water molecules [9–14]. Various surface pretreatment methods, such as carbon coating, chemical fluorination, oxidation, doping, etching, and acid treatments, are reported to improve the electrochemical characteristics of the active carbon material [13]. The surface treatment allows a more defined control in terms of surface chemistry, composition, and reactivity, eliminate surface functional groups and reduce the surface area and thereby reducing the irreversible capacity loss due to SEI formation [15,16].

Graphitic carbon material production requires expensive synthesis conditions and very high temperature treatments close to 3000 °C, to provide the mobility for carbon atoms to rearrange and crystallize carbon into a graphite structure [17]. However, carbon produced from waste tires requires a simple sulfonation process followed by pyrolysis in a nitrogen atmosphere at 1100 °C [18–22]. Sulfonated tire-derived carbons have been tested as anodes in a half-coin cell lithium-ion battery configuration [18]. This process needs to be scaled up and demonstrated in a pouch full-cell configuration. The waste tires as a raw material also add a high value to the end-of-life tire rubber and provide a sustainable solution to the huge amount of waste tires generated worldwide on an annual basis. The carbon production cost and energy savings can be less than half of the graphite production cost, due to low temperature pyrolysis and the availability of low-cost raw waste tire rubber material. The demand to produce new tires to meet the needs of the rapidly growing auto industry increased to 4.3 percent every year to 2.9 billion tires in 2017 [22]. This paper demonstrates the successful scale up production of carbon material in kg quantities with 20–40 μm size particles from waste tires and reported its electrochemical performances as a promising anode in both coin and pouch LIB cell configurations. The micronized carbon materials coated with a thin layer of carbon using a chemical vapor deposition (CVD) approach and investigated the effects of carbon coating towards the improvements in electrochemical performances in LIB cells is also reported. In addition, a simple prelithiation strategy to improve the first cycle efficiency to 94% is also presented.

2. Experimental

2.1. Material Synthesis

Tire rubber crumb of size 1.5 was soaked at 70 °C for 12 h in a concentrated sulfuric acid bath which yielded sulfonated rubber slurry [18]. The slurry was then filtered, washed, and pyrolyzed at 1100 °C. The furnace was ramped up from room temperature to 400 °C at a rate of 1 °C/min and further increased to 1100 °C at a rate of 2 °C/min and held for 2 h and then allowed to cool down to room temperature under flowing nitrogen gas. Similarly, the sulfonated slurry was also heated to 1400 °C. The carbon sample was removed and ground to 20–40 μm size particles and used for further studies [21]. The carbon sample was also coated with a thin layer of carbon using Toluene as an aromatic hydrocarbon feedstock in a fluidized bed chemical vapor deposition (CVD) reactor (see Figure 1) at 800 °C under flowing nitrogen. The Toluene source was kept at 70 °C and bubbled with nitrogen gas at a flow rate of 2 L/min for 30 min. The thickness of the carbon coating was 10-nm. The commercial graphite of ~20 μm size particles was obtained from MTI Corp., Richmond, CA, USA and used as a standard electrode material for comparison.

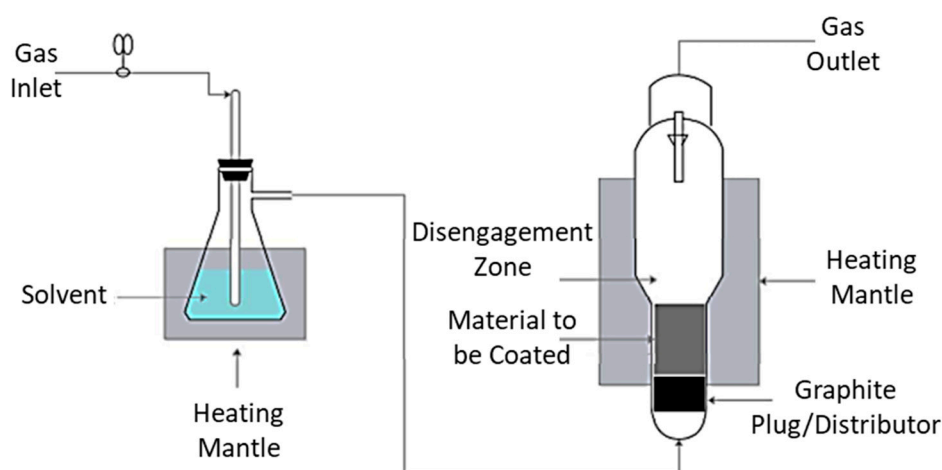


Figure 1. Schematic fluidized bed reactor for carbon coating.

2.2. Material Characterization

The carbon materials recovered from tires were characterized for their particle size, surface area, porosity, pore volume, morphology and crystallography. Nitrogen adsorption desorption isotherms were obtained with a Quantachrome NovaWin1000 Surface Area and Porosity Analyzer at 77.4 K. The specific surface area was determined by the Brunauer-Emmett-Teller (BET) method. The pore size distribution was obtained by the Barret-Joyner-Halenda (BJH) method. Raman spectra were collected with a Horiba LabRam HR using an excitation wavelength of 473 nm, a 600 g/mm grating and high spatial and spectral resolutions (800-mm monochromator). The X-ray powder diffraction (XRD) analysis was performed on a Rigaku Miniflex600 diffractometer with Cu K α radiation. A Zeiss Merlin VP scanning electron microscope (SEM), Thornwood, NY, USA operated at 3 kV was used to characterize the surface morphologies of the samples. Interlayer distances of the carbons were determined by a Hitachi HD-2300 A scanning transmission electron microscopy (STEM), Clarksburg, MD, USA with a field emission source operated at 200 kV in bright-field imaging mode at a 2.1 Å resolution.

2.3. Electrochemical Characterization of Half Cells

The electrode was prepared using a doctor blade coating technique by casting a slurry containing 80 wt % tire derived carbon material or graphite, 10 wt % conductive carbon (C-ENERGY Super C45,

Imerys Graphite & Carbon), and 10 wt % polyvinylidene difluoride (PVDF) binder in *n*-methyl-2-pyrrolidone (NMP) solvent onto a copper foil. The typical loading amount of active material was 2–2.5 mg/cm². The electrochemical performance and cycling tests were carried out in a CR2032 coin cell configuration. The coin cells were fabricated in an argon-filled glove box, using tire derived carbon with and without carbon coating or graphite electrode as the working electrode (10-mm diameter), metallic lithium foil as the counter electrode (13-mm diameter), Celgard 2325 as the separator and the solution of 1.0 M LiPF₆ in ethylene carbonate (EC)–dimethyl carbonate (DMC)–diethyl carbonate (DEC) (1:1:1 by volume) as the electrolyte. The coin cells were charge and discharge cycled using an Arbin BT2000 potentiostat/galvanostat multichannel system at room temperature under various constant current rates between C/5 (0.20 mA/cm²) and C/50 (0.02 mA/cm²) with the voltage cut off at 5 mV and 3.0 V.

2.4. Electrochemical Testing of Full Cells

The electrodes for pouch cells were made using a slot-die coater (Frontier Industrial Technology, Towanda, PA, USA) at Oak Ridge National Laboratory's (ORNL) Battery Manufacturing Facility (BMF) by following the coating procedures reported in detail elsewhere [23]. The cathode slurry contains 90% the active LiNi_{0.5}Mn_{0.3}Co_{0.2}O₂ (NMC532, Toda America, Battle Creek, MI, USA), 5% carbon black (Vulcan XR72C, Billerica, MA, USA), and 5% PVDF (PowerFlex, Kynar, Arkema Inc., Prussia, PA, USA) in NMP solvent. The anode slurry consists of 88% tire derived carbon material, 4% conductive carbon C45 and 8% PVDF binder (9300, Kureha America, New York, NY) in NMP solvent. The slurries were mixed separately in a high speed Ross planetary mixer (Charles Ross & Son Company, Hauppauge, NY, USA). The cathode and anode slurries were coated onto aluminum foil and copper foil respectively on a single side using the slot-die coater and transferred to a vacuum oven for drying at 120 °C overnight. A Celgard 2325 separator was used with an electrolyte composed of 1.2 M LiPF₆ in EC:DEC (3:7 wt ratio). The electrochemical performance characteristics and cycling tests were carried out in a pouch cell configuration. Pouch cells of dimensions: 84.4-mm long × 56.0-mm wide were fabricated in the dry room facility at BMF maintained at <0.5% (−53 °C dew point) humidity. The cycling performance tests were conducted at various charging and discharging current rates between C/5 and C/50 and the voltage between 2.0, 2.5 and 4.2 V using a potentiostat (VSP, BioLogic, Seyssinet-Pariset, France).

3. Results and Discussion

3.1. Material Characterization

Raman spectroscopy is being used as a nondestructive standard characterization tool to study crystalline, nanocrystalline, and amorphous carbons [24]. The position and width of the G and D bands and the intensity ratio of I_D/I_G are widely used for characterizing the degree of graphitization and the quantity of defects present in the graphitic materials [24–26]. The Raman spectra of commercial graphite exhibit a huge sharp G-band frequency centering at 1585 cm^{−1} and a small weak D-band at 1368 cm^{−1} (Figure 2a). The G peak is due to the bond stretching modes of all pairs of sp² atoms in both rings and chains. The D peak is due to the breathing modes of sp² atoms in the rings. The intensity ratio of I_D/I_G is calculated to be 0.123, with a small amount of disorder structure present in the commercial graphite compared to the perfect graphite where D band intensity is almost zero and therefore the ratio I_D/I_G = 0. The measured full-width-at-half-maximum (FWHM) of G band is 19.2 cm^{−1} compared to the perfect graphite which has 14 cm^{−1} on a basal plane and 18 cm^{−1} in the prismatic edges [26].

The Raman spectrum of tire derived carbon sample pyrolyzed at 1100 °C and 1400 °C shown in Figure 1b,c illustrate well-resolved two broad G and D bands. The carbon pyrolyzed at 1100 °C exhibits a broad G band centering at 1599 cm^{−1} and D band at 1363 cm^{−1} (Figure 2b) while pyrolyzed at 1400 °C exhibits also a broad G band centering at 1604 cm^{−1} and D band at 1363 cm^{−1} (Figure 2c); however the peaks in the sample pyrolyzed at 1400 °C are relatively narrower than those that in 1100 °C. The average

I_D/I_G ratio obtained are 0.86 and 0.99 and $\text{FWHM}(G)$ are 127 cm^{-1} and 89 cm^{-1} respectively for carbon pyrolyzed at both temperatures indicating a disorder crystalline structure [24,27]. The ratio of I_D/I_G is proportional to the number of aromatic rings. The increased relationship in the I_D/I_G ratio and G band position for the tire-derived carbons shows that more sp^2 amorphous carbon turns into nanocrystalline graphite at higher temperatures. The D band has a high sensitivity to disorder in the carbon material is usually attributed to the graphitization process and the formation of crystal growth [28]. This intensity of the D band increase through heat treatment could be related to the nano-crystallite graphite growth in the tire carbon caused by the defects and amorphous carbon.

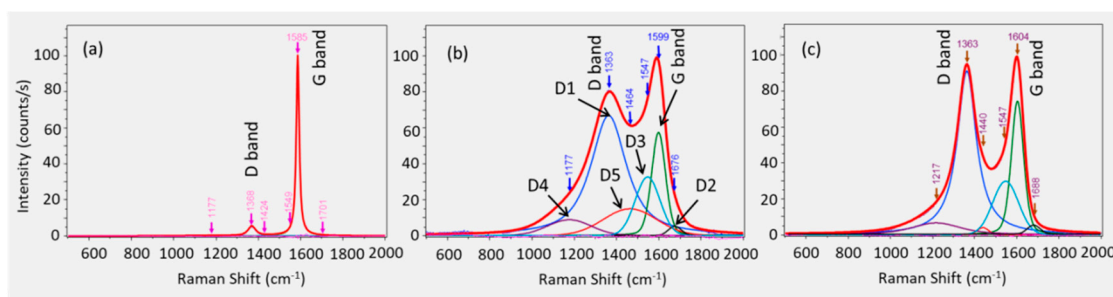


Figure 2. Raman spectra with peak deconvolution of (a) commercial graphite, and carbon produced from used tire with the pyrolysis temperatures of (b) $1100 \text{ }^\circ\text{C}$, and (c) $1400 \text{ }^\circ\text{C}$.

Deconvolution of the first order Raman spectrum of tire derived carbon pyrolyzed at $1100 \text{ }^\circ\text{C}$ was fitted with 6 curves attributed to the vibration modes of hexagonal carbon ring active at G-band (1599 cm^{-1}) represents an ideal graphitic structures, while D1 (1363 cm^{-1}), D2 (1676 cm^{-1}), D3 (1547 cm^{-1}), D4 (1177 cm^{-1}) and D5 (1464 cm^{-1}) bands relate to the defects in the disordered carbon structure (Figure 2b). Similarly, the tire derived carbon pyrolyzed at $1400 \text{ }^\circ\text{C}$ was also fitted with 6 curves: G-band (1603 cm^{-1}), D1 (1363 cm^{-1}), D2 (1688 cm^{-1}), D3 (1547 cm^{-1}), D4 (1217 cm^{-1}), and D5 (1440 cm^{-1}) (Figure 2c). The D1 band appears the most intense is normally assigned to the A_{1g} symmetry in the graphitic lattice vibration mode. The origin of the D1 band in disordered carbon is due to the vibration mode of large number of small graphitic crystallites in the polycrystalline tire derived carbon atoms, at the edge of the graphene layers [29,30]. Another feature observed in the spectra is related to the line broadening of the G and D1 bands, indicating that the distribution of phonons activated by disorder corresponds to crystallites of different sizes. The intensity of the D1 curve increased by 36% and G band by 29% and the FWHM is reduced for D1 and G bands by 45% for the sample pyrolyzed at $1400 \text{ }^\circ\text{C}$ compared to $1100 \text{ }^\circ\text{C}$ illustrating higher temperatures pyrolysis graphitizes the nanocrystals in a short range order and making it as disordered graphitic. Other defect bands D3 and D4 bands in carbon pyrolyzed at $1100 \text{ }^\circ\text{C}$ are assigned to the amorphous carbon and hydrocarbons connected to the basic structural units of graphitic carbon respectively [31,32]. The intensity of D3 and D4 curves are decreased by 10% and 25% respectively when the pyrolysis temperature increased from $1100 \text{ }^\circ\text{C}$ to $1400 \text{ }^\circ\text{C}$. The D5 band is detected at 1464 cm^{-1} for carbon pyrolyzed at $1100 \text{ }^\circ\text{C}$ and 1440 cm^{-1} for carbon pyrolyzed at $1400 \text{ }^\circ\text{C}$ assigned to hydrocarbons trapped in the carbon pores [33].

Figure 3a illustrates a low magnification scanning electron microscopy (SEM) image of tire derived carbon particles of various micron sizes and shapes with macro- and meso-pores visible on the sample surface. Figure 3b illustrates the high-resolution scanning transmission electron microscopy (HR-STEM) image of uncoated carbon pyrolyzed at $1100 \text{ }^\circ\text{C}$, of both graphite layers and amorphous carbon phase pattern. Figure 3c illustrates a cross-sectional layered structure of carbon with the contrast profile of $\sim 4.5 \text{ \AA}$ interlayer spacing. Figure 3d illustrates the selected area electron diffraction (SAED) patterns of uncoated carbon showing the coexistence of short range ordered graphite phase and amorphous regions. The fringes represent the stacks of graphene layers of polyaromatic structures [34].

These fringes are very short and completely disoriented. Figure 3e illustrates a HR-STEM image of carbon coated tire derived carbon, showing a uniform carbon coating of ~ 10 nm thickness on the surface of the carbon. The carbon coating enables the reduction of the surface area from 110 to 20 m^2/g .

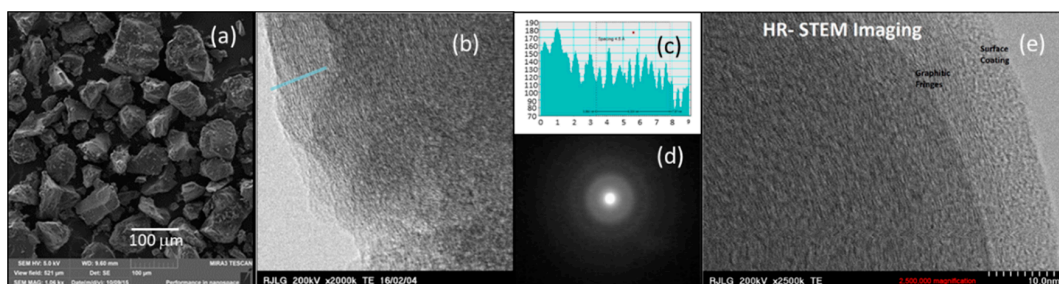


Figure 3. Tire derived carbon (a) scanning electron microscope (SEM) image, (b) high-resolution scanning transmission electron microscopy (HR-STEM) images showing both planar and cross-sectional layered structures, (c) the contrast profile of ~ 4.5 Å spacings, (d) Selected Area Electron Diffraction pattern (SAED), and (e) HR-STEM image of carbon coated tire derived carbon.

X-ray photoemission spectroscopy (XPS) spectra of the tire-derived carbons are shown in Figure 4. The C1s spectra in Figure 4a for both carbon samples of carbon coated and uncoated show a sharp peak at 284.8 eV, which is due to the sp^2 configuration. The fitting results for C1s spectra show that the Carbon peak is narrow consistent with C-C bond and there are no C-O or C=O groups on the surface. Figure 4b shows the S2p scans of the samples. The peak at about 164 eV is related to the thiol group. A small doublet spike at around 165.2 eV could be due to the trace amount of sulfate group present. It was shown that the sulfate groups are completely removed from the sample when the pyrolysis temperature is increased further to 1600 °C [22]. The XPS elemental analysis for the samples is shown in Table 1. The carbon coating increases the carbon percentage by 4.7% while the O2s and S2p are reduced by 16.78% and 0.84%, respectively.

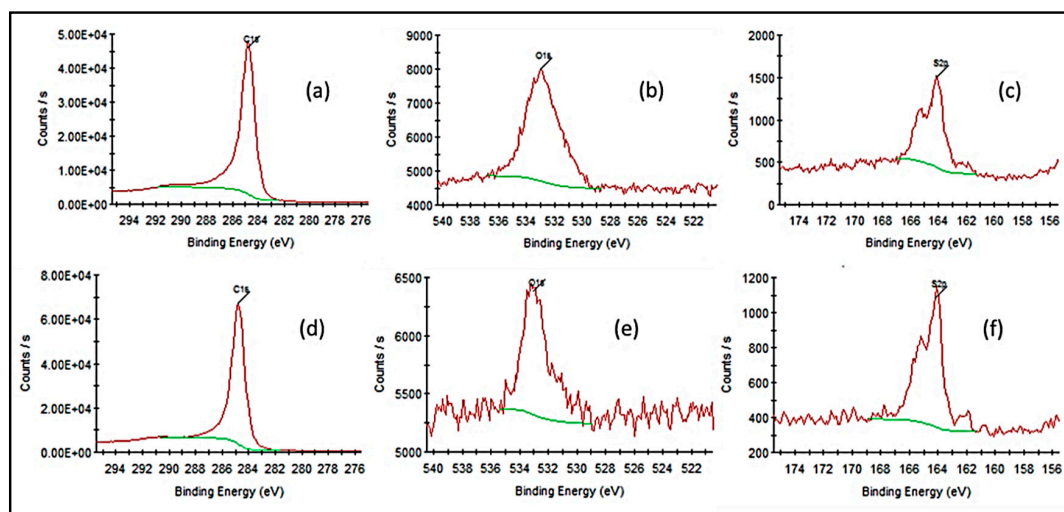


Figure 4. X-ray photoelectron spectroscopy (XPS) data of tire derived carbon, uncoated (top), and carbon coated (bottom) of scans of (a,d) C1s, (b,e) O2s, and (c,f) S2p.

Material characterization studies clearly demonstrate that the carbon material synthesized from waste tires has a unique disordered nanoporous structure with a large interlayer distance than that of graphite. This novel carbon material synthesis technology from tires demonstrates more sustainable and efficient use of resources.

Table 1. XPS surface concentration (in atomic percentages) of coated and uncoated tire derived carbon samples.

XPS Scans	Atomic %		Peak BE		FWHM eV		Area (P) CPS eV		SF	
	Coated	Uncoated	Coated	Uncoated	Coated	Uncoated	Coated	Uncoated	Coated	Uncoated
C1s	97.82	93.3	284.79	284.79	1.10	1.15	87,813.38	69,670.55	1	1
O2s	1.23	5.2	533.02	532.9	1.77	2.67	2701.93	9541.84	2.93	2.93
S2p	0.96	1.5	164.19	164.19	1.03	0.91	1546.58	2012.37	1.67	1.67

3.2. Electrochemical Measurements of Half Cells

Uncoated carbon materials of 38 μm and 20 μm particle sizes and carbon coated carbon materials of 20 μm particle size were utilized in half coin cells having lithium metal as the counter electrode in standard electrolyte solutions were cycled at various current rates are presented in Figure 5. The cell with larger particle size (38 μm) exhibited an initial first cycle coulombic efficiency of 51% at C/3 charge/discharge current rate. The first cycle coulombic efficiency was increased to 60% when the starting particle size was reduced to 20 μm and to 66% for carbon coated tire derived carbon samples. Further cycling exhibited the coulombic efficiency close to 100% for all the samples. The reversible capacity of uncoated carbon material is 247 mAh/g at C/5 charge/discharge current rate and it increased to 364 mAh/g for smaller size particles (20 μm) and it increased further to 437 mAh/g with carbon coated sample. Lowering the charge discharge cycling rate to C/7.5 and C/50 also increased the reversible capacity to 300 mAh/g and 430 mAh/g respectively corresponding to 65% and 92% respectively to the first cycle capacity. These results are interesting because the lithium utilization at C/50 current rate cycling is 92% which means the actual irreversible capacity loss is only 8%. This indicates that the apparent first cycle irreversible capacity loss was not due to the SEI formation rather it is related to the polarization caused by the poor conductivity of the carbon material. When the carbon was coated with a thin layer of carbon the capacity increased to 432 mAh/g at C/10 current rate. The increased capacity for the carbon coated sample can be related to the increased conductivity due to high carbon concentration of 98% and lower oxygen percentage of 1.23% as found from XPS studies (Table 1).

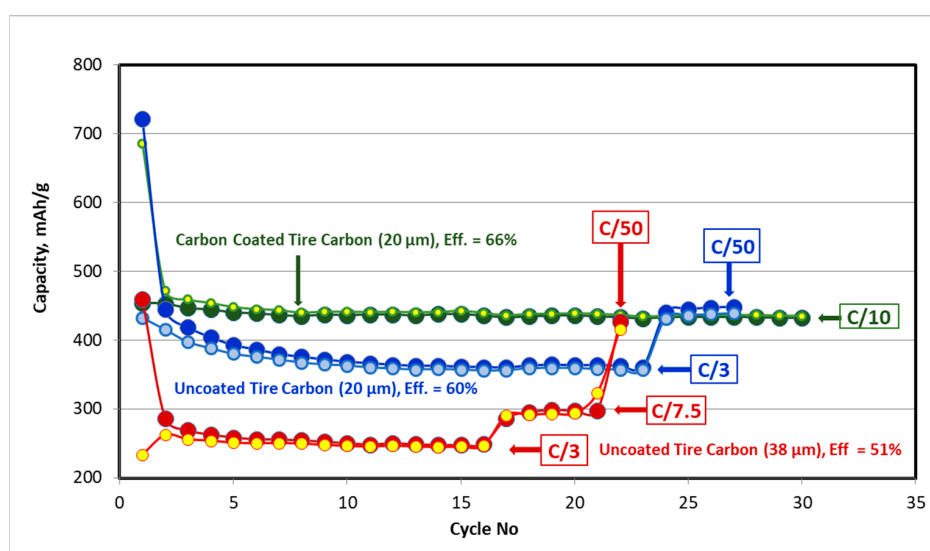
**Figure 5.** Cycling performance of lithium ion coin cells having lithium metal foil as the counter electrode and uncoated tire derived carbon of 38 μm and 20 μm size particle size and carbon coated tire derived carbon of 20 μm size particles cycled at various current rates.

Figure 6 compares charge capacities of uncoated and carbon coated tire derived carbon electrode material of 20 μm particle size pyrolyzed at 1100 $^{\circ}\text{C}$ and commercial graphite (20 μm) working electrodes in half coin cells. The uncoated carbon electrode exhibited 364 mAh/g capacity which is 3% higher capacity than that of the commercial graphite (353 mAh/g) while carbon coated exhibited 20% higher capacity of 437 mAh/g. The carbon coating also improved the first cycle columbic efficiency by 10%. The irreversible capacity and the surface area of the active material are directly proportional (higher capacity for low surface area of 20 m^2/g with carbon coated samples compared to the lower capacity for high surface area of 110 m^2/g with uncoated carbon samples).

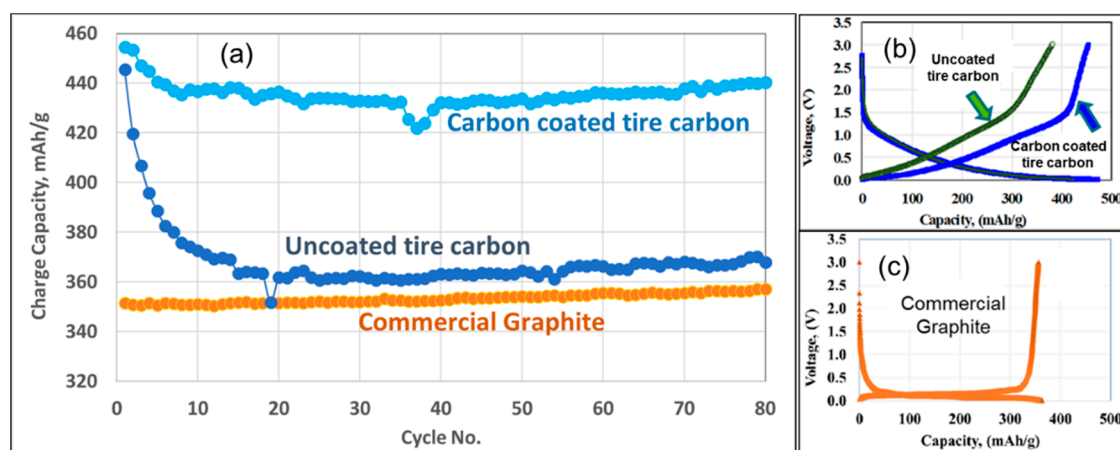


Figure 6. Comparison of cycling performances of uncoated and carbon coated tire derived carbon with commercial graphite as working electrodes vs. lithium metal counter electrode: (a) capacity plot, and (b,c) voltage profiles.

The carbon coating also reduced the interfacial resistance between the particles and improved the surface conductivity and thus enhanced the reversible capacity [11]. Furthermore, the carbon coating has reduced the voltage hysteresis in carbon coated samples (Figure 6b) compared to the uncoated carbon sample. The difference in the charge discharge voltage behavior of graphite (Figure 6c) vs. the carbons was found to correlate well with their unique structure [8]. The lithium insertion mechanism at higher voltage starting from ~ 1.2 V is more of an adsorption behavior while an intercalation process occurs at lower voltages [8,9]. The carbons vs. Li counter electrodes in coin-type cells reveal exceptionally good cycleability, with only moderate capacity fading.

3.3. Electrochemical Measurements of Pouch Full Cells

The use of tire derived carbon as a promising anode material in a lithium-ion battery pouch full cell configuration having NMC532 as cathode in standard electrolyte solutions has been demonstrated in Figure 7. The formation cycling tests were first performed at C/5, C/20, and C/50 charge and discharge current rates. After the formation cycling, the cells were cycled at C/5 charge discharge rate lost 0.12% capacity per cycles when the voltage cut off was limited to 2.0 V while the rest of the cycles lost only 0.08% capacity per cycle at 2.5 V limit. After 160 cycles at C/5, the cells were further cycled at lower current rate of C/50 showed an increase of 12% in reversible capacity. The cycling tests demonstrate carbon as a promising anode material in full cell configuration. Further electrochemical characterizations were carried out to design better cell chemistry.

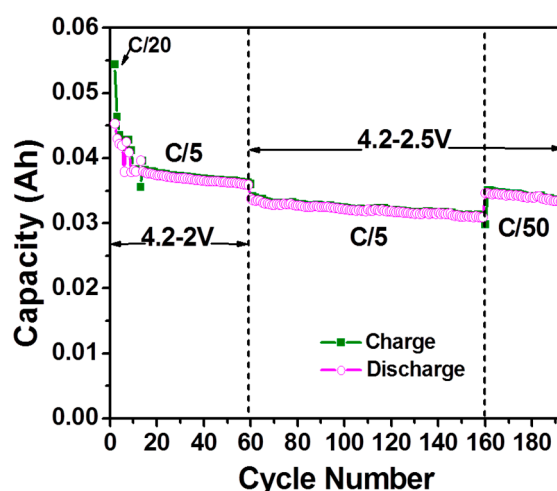


Figure 7. Cycling performance of the carbon anode material pyrolyzed at 1100 °C vs. NMC532 cathode at various current rates.

3.4. Prelithiation of Carbon Anodes

Prelithiation is an important strategy that attracts more and more interest to compensate for lithium loss in the formation cycle in lithium-ion batteries. Experimentally, it is more challenging to pre-lithiate anode materials than to pre-lithiate cathode materials since it requires a more reactive lithium source and the process is hard to control. There are some reports using stabilized lithium metal powder (SLMP), however, this type of material is expensive and hard to disperse in NMP solution during the slurry preparation [35–37]. It will require a special complex procedure to apply pre-lithiated anodes.

The goal of using pre-lithiation treatment is to achieve first cycle efficiency of over 90% for the electrode materials. Here, the pre-lithiation is conducted by direct contacting of lithium metal with the electrolyte wetted with casted electrode, as shown in Figure 8a [38]. Different contact periods were studied to optimize the process conditions. Since the electrode was shorted after contact with Li, the assembled cell has almost 0 V OCV and at this time, first cycle efficiency would be that of the real second cycle since the first discharge is skipped. It is noticeable that all pre-lithiated cells have a very high efficiency (over 94%) from the beginning, compared to 60% efficiency of the cell without pre-lithiation. There are no major differences in the electrochemical performances during the first 22 cycles for different pre-lithiated electrodes shown in Figure 8. However, the long-term cycling test is needed to fully evaluate the influence of electrode properties.

In the meantime, new methods could be developed to pre-lithiate electrode materials, and they might be conducted in the future. Half cells with electrodes could be assembled and discharged to certain voltage, followed by disassembling of the cell and washing of the electrodes, then full cells can be made with pre-lithiated electrodes. This method can precisely control the amount of lithium pre-intercalated into the electrodes. Another approach is to use Li_3N as a lithium source additive when preparing the slurry and make a pouch cell [39]. Li_3N will decompose at 0.44 V during the formation cycle and the N_2 gas generated could be released before the final sealing of the pouch cell. Successful implementation of this technology would result in a significant reduction in carbon emissions and possibly result in a lower-cost higher performance lithium-ion battery [40–45].

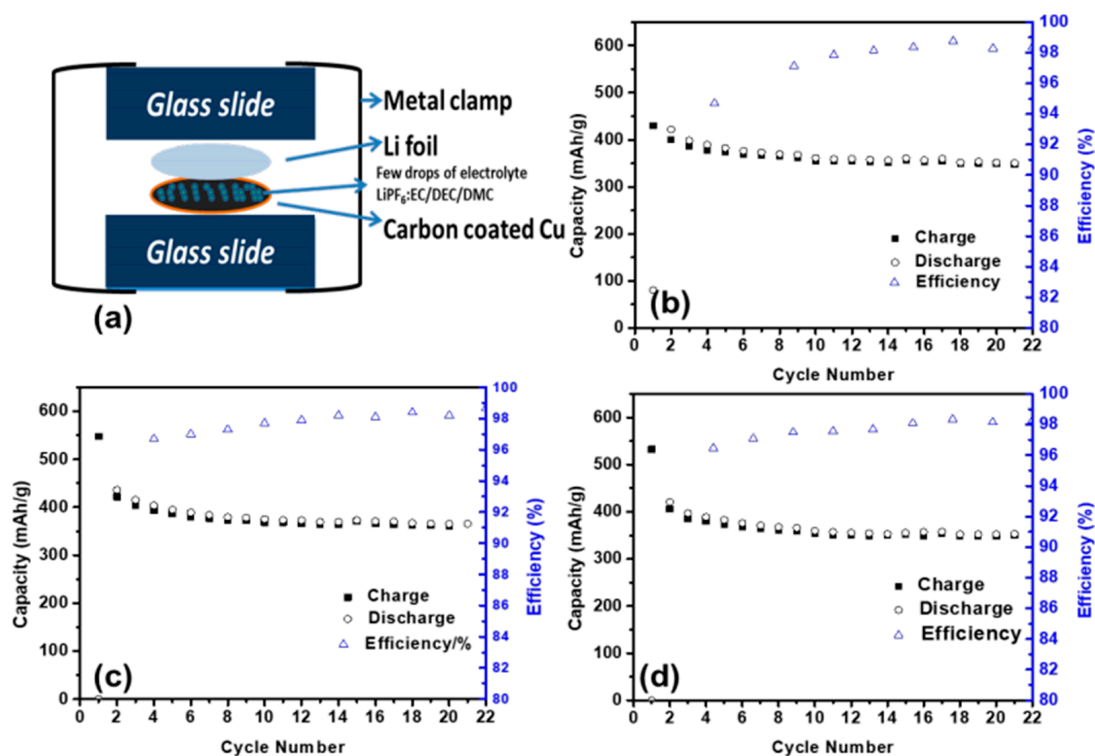


Figure 8. (a) Schematic of direct contact pre-lithiation process, electrochemical test data with (b) 20 min, (c) 19 h, (d) 23 h contact.

4. Conclusions

In summary, battery grade tire-derived carbon material was successfully prepared in high purity in large quantities and demonstrated as a potential anode material for LIBs. The combustion of waste tire rubber produces lower fossil CO₂ emissions per unit of energy (136.51 gCO₂/kW·h) compared to other conventional fossil fuels such as coal or fuel–oil, usually used in power generation [40]. The surface coating of the carbon improved the reversible lithium capacity by 20% and yielded 437 mAh/g, which is 20% higher than that of the commercial graphite. A novel prelithiation approach also yielded the first cycle efficiency of 94%. This novel green process can promote environmental sustainability to add value to the waste tires and benefit the battery industry to solve future energy crises.

Author Contributions: J.S.G. planned the experiments and wrote the paper, R.J.L., and A.M.L. identified the research questions, J.L.W., and S.L.W. carried out scale up carbon material synthesis, Y.L., J.L., and K.A. carried out the experimental work, A.K.N. and M.P.P. came up with the concept and analyzed the data.

Acknowledgments: The research (Y.L., M.P.P.) was supported by the U.S. Department of Energy (DOE), Office of Science, Office of Basic Energy Sciences, Materials Sciences and Engineering Division. Part of research at RJ Lee Group was funded by internal funding.

Conflicts of Interest: The authors declare no competing financial interest.

Notice: UT-Battelle: LLC under Contract No. DE-AC05-00OR22725 with the DOE authored this manuscript. The United States Government retains and the publisher, by accepting the article for publication, acknowledges that the United States Government retains a non-exclusive, paid-up, irrevocable, world-wide license to publish or reproduce the published form of this manuscript, or allow others to do so, for United States Government purposes. The DOE will provide public access to these results of federally sponsored research in accordance with its Public Access Plan (<http://energy.gov/downloads/doe-public-access-plan>).

References

1. Diouf, B.; Pode, R. Potential of lithium-ion batteries in renewable energy. *Renew. Energy* **2015**, *76*, 375–380. [[CrossRef](#)]
2. Novák, P.; Goers, D.; Spahr, M.E. Carbon Materials in Lithium-Ion Batteries. In *Carbons for Electrochemical Energy Storage Systems*; Beguin, F., Frackowiak, E., Eds.; CRC Press: Boca Raton, FL, USA, 2010; Chapter 7, pp. 263–328, ISBN 978-1-4200-5307-4.
3. Battery University, Safety of Lithium-ion Batteries. 2017. Available online: http://batteryuniversity.com/learn/article/safety_of_lithium_ion_batteries (accessed on 2 June 2017).
4. Hori, H.; Shikano, M.; Kobayashi, H.; Koike, S.; Sakaebe, H.; Saito, Y.; Tatsumi, K.; Yoshikawa, H.; Ikenaga, E. Analysis of hard carbon for lithium-ion batteries by hard X-ray photoelectron spectroscopy. *J. Power Sources* **2013**, *242*, 844–847. [[CrossRef](#)]
5. Shi, H. Coke vs. graphite as anodes for lithium-ion batteries. *J. Power Sources* **1998**, *75*, 64–72. [[CrossRef](#)]
6. Buiel, E.; Dahn, J.R. Li-insertion in hard carbon anode materials for Li-ion batteries. *Electrochim. Acta* **1999**, *45*, 121–130. [[CrossRef](#)]
7. Gnanaraj, J.S.; Levi, M.D.; Levi, E.; Salitra, G.; Aurbach, D.; Fischer, J.E.; Claye, A. Comparison Between the Electrochemical Behavior of Disordered Carbons and Graphite Electrodes in Connection with Their Structure. *J. Electrochem. Soc.* **2001**, *148*, A525–A536. [[CrossRef](#)]
8. Dahn, J.R.; Zheng, T.; Liu, Y.; Xue, J.S. Mechanisms for Lithium Insertion in Carbonaceous Materials. *Science* **1995**, *270*, 590–593. [[CrossRef](#)]
9. Peled, E. The Electrochemical Behavior of Alkali and Alkaline Earth Metals in Nonaqueous Battery Systems—The Solid Electrolyte Interphase Model. *J. Electrochem. Soc.* **1979**, *126*, 2047–2051. [[CrossRef](#)]
10. Gnanaraj, J.S.; Thompson, R.W.; Iaconatti, S.N.; DiCarlo, J.F.; Abraham, K.M. Formation and Growth of Surface Films on Graphitic Anode Materials for Li-Ion Batteries. *Electrochem. Solid-State Lett.* **2005**, *8*, A128–A132. [[CrossRef](#)]
11. Lee, J.H.; Lee, H.Y.; Oh, S.M.; Lee, S.J.; Lee, K.Y.; Lee, S.M. Effect of carbon coating on electrochemical performance of hard carbons as anode materials for lithium-ion batteries. *J. Power Sources* **2007**, *166*, 250–254. [[CrossRef](#)]
12. Guerin, K.; Fevrier-Bouvier, A.; Flandrois, S.; Simon, B.; Biensan, P. On the irreversible capacities of disordered carbons in lithium-ion rechargeable batteries. *Electrochim. Acta* **2000**, *45*, 1607–1615. [[CrossRef](#)]
13. Kumar, T.P.; Kumari, T.S.D.; Stephan, A.M. Carbonaceous anode materials for lithium-ion batteries—the road ahead. *J. Ind. Inst. Sci.* **2009**, *89*, 393–424.
14. Xing, W.; Dahn, J.R. Study of irreversible capacities for Li insertion in hard and graphitic carbons. *J. Electrochem. Soc.* **1997**, *144*, 1195–1201. [[CrossRef](#)]
15. Xu, K. Electrolytes and Interphases in Li-Ion Batteries and Beyond. *Chem. Rev.* **2014**, *114*, 11503–11618. [[CrossRef](#)] [[PubMed](#)]
16. Buiel, E.; Dahn, J.R. Reduction of the Irreversible Capacity in Hard-Carbon Anode Materials Prepared from Sucrose for Li-Ion Batteries. *J. Electrochem. Soc.* **1998**, *145*, 1977–1981. [[CrossRef](#)]
17. Tamashauskay, A.V. *An Introduction to Synthetic Graphite*; Asbury Graphite Mills Inc.: Pittsburgh, PA, USA, 2006; Available online: <https://asbury.com/pdf/SyntheticGraphitePartI.pdf> (accessed on 12 April 2018).
18. Naskar, A.K.; Bi, Z.; Li, Y.; Akato, S.K.; Saha, D.; Chi, M.; Bridges, C.A.; Paranthaman, M.P. Tailored recovery of carbons from waste tires for enhanced performance as anodes in lithium-ion batteries. *RSC Adv.* **2014**, *4*, 38213–38221. [[CrossRef](#)]
19. Naskar, A.K.; Paranthaman, M.P.; Bi, Z. Pyrolytic Carbon Black Composite and Method of Making the Same. U.S. Patent 9,441,113 B2, 13 September 2016.
20. Boota, M.; Paranthaman, M.P.; Naskar, A.K.; Li, Y.; Akato, K.; Gogotsi, Y. Waste Tire Derived Carbon—Polymer Composite Paper as Pseudocapacitive Electrode with Long Cycle Life. *ChemSusChem* **2015**, *8*, 3576–3581. [[CrossRef](#)] [[PubMed](#)]
21. Gnanaraj, J.S.; Lee, R.J.; Levine, A.M.; Wistrom, J.L.; Wistrom, S.L.; Li, Y.; Li, J.; Naskar, A.K.; Paranthaman, M.P. A Low-Cost Carbon Composite Anode Material from Recycled Waste Tires for Lithium-Ion Batteries. In Proceedings of the MRS Spring Meeting & Exhibit about Symposium EE4—Electrode Materials and Electrolytes for Lithium and Sodium Ion Batteries, Phoenix, AZ, USA, 28 March–1 April 2016. Paper EE4.5.06.

22. Li, Y.; Paranthaman, M.P.; Akato, K.; Naskar, A.K.; Levine, A.M.; Lee, R.J.; Kim, S.; Zhang, J.; Dai, S.; Manthiram, A. Tire-derived Carbon Composite Anodes for Sodium-ion Batteries. *J. Power Sources* **2016**, *316*, 232–238. [[CrossRef](#)]
23. Li, J.; Daniel, C.; An, S.J.; Wood, D. Evaluation residual moisture in lithium-ion battery electrodes and its effect on electrode performance. *MRS Adv.* **2016**, *1*, 1029–1035. [[CrossRef](#)]
24. Ferrari, A.C.; Robertson, J. Interpretation of Raman spectra of disordered and amorphous carbon. *Phys. Rev. B* **2000**, *61*, 14095. [[CrossRef](#)]
25. Manoj, B.; Kunjomana, A.G. Chemical leaching of an Indian bituminous coal and characterization of the products by vibrational spectroscopic techniques. *Int. J. Miner. Metall. Mater.* **2012**, *19*, 279–283. [[CrossRef](#)]
26. Maslova, O.A.; Ammar, M.R.; Guimbretière, G.; Rouzaud, J.-N.; Simon, P. Determination of crystallite size in polished graphitized carbon by Raman spectroscopy. *Phys. Rev. B* **2012**, *86*, 134205. [[CrossRef](#)]
27. Ferrari, A.C.; Robertson, J. Raman spectroscopy of amorphous, nanostructured, diamond-like carbon, and nanodiamond. *Phil. Trans. R. Soc. Lond. A* **2004**, *362*, 2477–2512. [[CrossRef](#)] [[PubMed](#)]
28. Deldicque, D.; Rouzaud, J.-N.; Velde, B.; Raman, A. A Raman—HRTEM study of the carbonization of wood: A new Raman-based paleothermometer dedicated to archaeometry. *Carbon* **2016**, *102*, 319–329. [[CrossRef](#)]
29. Manoj, B.; Kunjomana, A.G. Study of Stacking Structure of Amorphous Carbon by X-Ray Diffraction Technique. *Int. J. Electrochem. Sci.* **2012**, *7*, 3127–3134.
30. Zhou, Q.; Zhao, Z.; Zhang, Y.; Meng, B.; Zhou, A.; Qiu, J. Graphene Sheets from Graphitized Anthracite Coal: Preparation, Decoration, and Application. *Energy Fuels* **2012**, *26*, 5186–5192. [[CrossRef](#)]
31. Sadezky, A.; Muckenhuber, H.; Grothe, H.; Niessner, R.; Pöschl, U. Raman spectroscopy of soot and related carbonaceous materials: Spectral analysis and structural information. *Carbon* **2005**, *43*, 1731–1742. [[CrossRef](#)]
32. Pawlyta, M.; Rouzaud, J.N.; Duber, S. Raman microspectroscopy characterization of carbon black: Spectral analysis and structural information. *Carbon* **2015**, *84*, 479–490. [[CrossRef](#)]
33. Ramya, A.V.; Manoj, B.; Mohan, A.N. Extraction and characterization of wrinkled graphene nanolayers from commercial graphite. *Asian J. Chem.* **2016**, *28*, 1031–1034. [[CrossRef](#)]
34. Rosalin, F. Crystallite Growth in Graphitizing and Non-Graphitizing Carbons. *Proc. R. Soc. Lond.* **1951**, *209*, 196–218. [[CrossRef](#)]
35. Forney, M.W.; Ganter, M.J.; Staub, J.W.; Ridgley, R.D.; Land, B.J. Prelithiation of Silicon–Carbon Nanotube Anodes for Lithium Ion Batteries by Stabilized Lithium Metal Powder (SLMP). *Nano Lett.* **2013**, *13*, 4158–4163. [[CrossRef](#)] [[PubMed](#)]
36. Wang, Z.; Fu, Y.; Zhang, Z.; Yuan, S.; Amine, K.; Battaglia, V.; Liu, G. Application of Stabilized Lithium Metal Powder (SLMP) in graphite anode—A high efficient prelithiation method for lithium-ion batteries. *J. Power Sources* **2014**, *260*, 57–61. [[CrossRef](#)]
37. Jarvis, C.R.; Lain, M.J.; Yakovleva, M.V.; Gao, Y. A prelithiated carbon anode for lithium-ion battery applications. *J. Power Sources* **2006**, *162*, 800–802. [[CrossRef](#)]
38. Liu, N.; Hu, L.; McDowell, M.T.; Jackson, A.; Cui, Y. Prelithiated Silicon Nanowires as an Anode for Lithium Ion Batteries. *ACS Nano* **2011**, *5*, 6487–6493. [[CrossRef](#)] [[PubMed](#)]
39. Park, K.; Yu, B.-C.; Goodenough, J.B. Cathode Additive for High-Energy-Density Lithium-Ion Batteries. *Adv. Energy Mater.* **2016**, *6*, 2534. [[CrossRef](#)]
40. Martinez, J.D.; Puy, N.; Murillo, R.; Garcia, T.; Navarro, M.V.; Mastral, A.M. Waste tyre pyrolysis—A review. *Renew. Sustain. Energy Rev.* **2013**, *23*, 179–213. [[CrossRef](#)]
41. Li, J.; Qian, Y.; Wang, L.; He, X. Nitrogen-Doped Carbon for Red Phosphorous Based Anode Materials for Lithium Ion Batteries. *Materials* **2018**, *11*, 134. [[CrossRef](#)] [[PubMed](#)]
42. Zhou, Y.; Wang, Q.; Zhu, X.; Jiang, F. Three-Dimensional SnS Decorated Carbon Nano-Networks as Anode Materials for Lithium and Sodium Ion Batteries. *Nanomaterials* **2018**, *8*, 135. [[CrossRef](#)] [[PubMed](#)]
43. Yuan, G.; Xiang, J.; Jin, H.; Wu, L.; Jin, Y.; Zhao, Y. Anchoring ZnO Nanoparticles in Nitrogen-Doped Graphene Sheets as a High-Performance Anode Material for Lithium-Ion Batteries. *Materials* **2018**, *11*, 96. [[CrossRef](#)] [[PubMed](#)]

44. Li, H.; Liu, Z.; Yang, S.; Zhao, Y.; Feng, Y.; Bakenov, Z.; Zhang, C.; Yin, F. Facile Synthesis of ZnO Nanoparticles on Nitrogen-Doped Carbon Nanotubes as High-Performance Anode Material for Lithium-Ion Batteries. *Materials* **2017**, *10*, 1102. [[CrossRef](#)] [[PubMed](#)]
45. Hwang, J.; Ihm, J.; Lee, K.-R.; Kim, S. Computational Evaluation of Amorphous Carbon Coating for Durable Silicon Anodes for Lithium-Ion Batteries. *Nanomaterials* **2015**, *5*, 1654–1666. [[CrossRef](#)] [[PubMed](#)]



© 2018 by the authors. Licensee MDPI, Basel, Switzerland. This article is an open access article distributed under the terms and conditions of the Creative Commons Attribution (CC BY) license (<http://creativecommons.org/licenses/by/4.0/>).